Hindawi Publishing Corporation
Research Letters in Physical Chemistry
Volume 2007, Article ID 32528, 5 pages
doi:10.1155/2007/32528

Research Letter

Anisotropic Vanadium Oxide Nanostructured Host Matrices for Lithium Ion Intercalation

C. O'Dwyer,[1] V. Lavayen,[1,2] M. A. Santa Ana,[2] E. Benavente,[3] G. González,[2] and C. M. Sotomayor Torres[1,4,5]

[1] *Tyndall National Institute, University College Cork, Cork, Ireland*
[2] *Department of Chemistry, Faculty of Science, University of Chile, Santiago, Chile*
[3] *Department of Chemistry, Universidad Tecnológica Metropolitana, Santiago, Chile*
[4] *Institute for Research and Advanced Studies, ICREA, 08010 Barcelona, Spain*
[5] *Catalan Institute of Nanotechnology, Autonomous University of Barcelona, Edifici CM7, Bellaterra, 08193 Barcelona, Spain*

Correspondence should be addressed to C. O'Dwyer, colm.odwyer@tyndall.ie

Received 26 June 2007; Accepted 6 August 2007

Recommended by David L. Andrews

We report on unique high-volume low-dimensional V_2O_5-based turbostratic nanostructures, prepared using sol-gel synthetic methods from $V_2O_5 \cdot nH_2O$ xerogels. Electrochemical intercalation of Li^+ to form $Li_{0.65}V_2O_5$ resulted in a maximum measured charge capacity of 1225 mAh g^{-1} as the β-$Li_xV_2O_5$ phase. Conductivities of the order of 10^{-3} S cm^{-1} were found on compressed-nanotube parallelepipedal samples, which exhibit an anisotropy factor of 70 at room temperature by preferential alignment of the nanotubes. The improved electrochemical properties observed in novel vanadium oxide nanostructured arrays are attributed to the increased volumetric density for ion intercalation, shorter diffusion paths to the intercalation sites, and a high degree of crystallinity of the individual nanotubular host structures.

1. INTRODUCTION

It is critical that low-cost, lightweight, small-volume, and environment friendly energy storage/conversion devices are developed, and nanomaterials are attracting great interest for electrochemical energy storage, for example, in rechargeable lithium ion battery technologies.

Vanadium pentoxide is a typical intercalation compound as a result of its layered structure [1]. The intercalation reactions involving layered host lattices have been most extensively studied because of their structural flexibility and ability to adapt to the geometry of the intercalated guest species by free adjustment of the interlaminar separation [2, 3].

The focus of this Letter concerns lithium ion intercalation properties of novel vanadium pentoxide nanostructures, by employing synthetic methods of preparing unique high-volume low-dimensional V_2O_5-based turbostratic morphologies. It is the uncomplicated sol-gel synthesis method in combination with structurally directing organic templates and hydrothermal treatment that produces the most desirable structures with remarkable regularity, reliability, efficiency, selectivity, and variety. Electrical and electrochemical studies of lithium intercalation reveal that these V_2O_5 nanostructures are redox active and readily undergo reversible reactions with lithium ions [4], resulting in remarkably high charge capacities. In addition, the various architectures are comprised of nanotubular V_2O_5 structures [5], which act as electrolyte-filled channels for faster transport of ions to intercalation sites. We also present observations on how a phase change structure polymorphism of the host influences the discharging characteristics.

2. EXPERIMENTAL

2.1. Synthesis of Vanadium Oxide Nanostructures

The method employed for the synthesis of vanadium pentoxide nanotubes and nanourchin have been previously outlined elsewhere [6–10]. Vanadium pentoxide nanorods were obtained by the following procedure: an aqueous solution of NH_4VO_3 was mixed with hexadecylamine (HDA) in a molar ratio of 2 : 1 under vigorous stirring. The hydrothermal treatment (HT) of the yellow suspension was performed in a Teflon-lined autoclave at 453 K for 4 days.

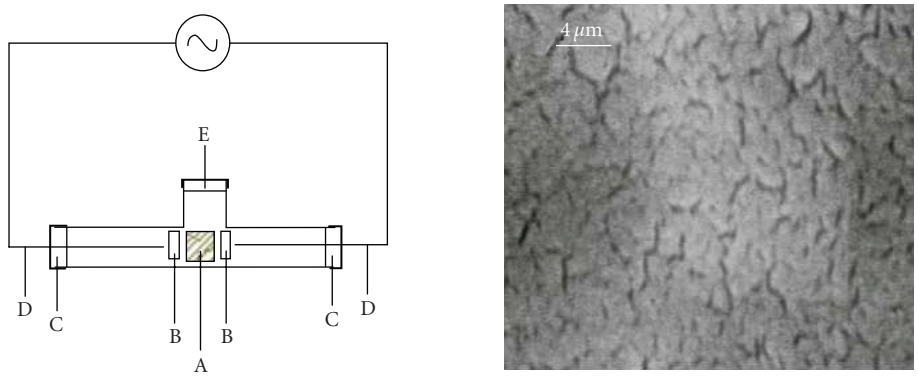

(a) (b)

Figure 1: (a) Schematic of the symmetrical cell four-point probe arrangement for conductivity measurements as a function of temperature. (A) compressed nanotubes sample, (B) gold contact, (C) hermetic latex seals, (D) point probes, (E) latex seal connected to Ar supply. (b) FESEM image of the surface of the compressed pill.

2.2. Methods of characterization

The morphological characterization of the nanostructured products was performed by field emission scanning electron microscopy (FESEM) using a JEOL JSM-6700F FESEM operating at beam voltages in the range 1–10 kV. Electron transparent specimens were prepared by ion-milling techniques and placed on a holey carbon support. Transmission electron microscopy (TEM) and selected area electron diffraction (SAED) were conducted using a Philips CM300 FEGTEM operating at 300 kV.

Conductivity measurements were performed on compressed-nanotube parallelepipedal samples in a hermetically sealed chamber in an argon atmosphere, shown in Figure 1. The electrical measurements were performed with an electrochemical impedance analyzer PAR model 6310, using ion blocking electrodes realized by sputtering a film of ∼30 nm of gold on opposite faces of the pellets, in the temperature range 298–343 K by applying an alternating voltage of amplitude 0.01 V over the frequency range 10^6–10^{-1} Hz.

The coulometric titration for intercalation of lithium into $V_2O_5 \cdot 1.5H_2O(HDA)_{0.7}$ was carried out in an electrochemical cell containing 0.5 mol dm^{-3} $LiCF_3SO_3$ (Frederick Smith Chemical Co.) in propylene carbonate-ethylene carbonate (molar ratio of 1 : 1) mixed with V_2O_5 nanotubes at a constant current density of 150 mA cm^{-2} represented as Li|PEO-$LICF_3SO_3$|$Li_xV_2O_5$, C, PEO. The V_2O_5 nanotube cathode was prepared by pressing a powder mixture of $V_2O_5 \cdot 1.5H_2O(HDA)_{0.7}$ and graphite (10%) in a steel template under a pressure of 2.3 MPa.

3. RESULTS AND DISCUSSION

3.1. Macroscopic ordering of V_2O_5 nanostructures

Typical FESEM and TEM micrographs of the nanostructured V_2O_5 products are shown in Figure 2. Considering the high degree of anisotropy in the nanotubular structures, experiments directed to attain macroscopic ordering were performed by pressing the powders into the form of special die. We have recently demonstrated that the resulting parallelepipedal pellets clearly show morphological, structural, as well as electrical anisotropic properties [11].

X-ray powder diffraction patterns of V_2O_5-based nanocomposites are shown in Figure 3. Each of the nanostructured products stemmed from the same precursor, and diffraction data were acquired after surfactant template intercalation and HT. All X-ray spectra exhibited a deviation in relative peak intensity compared to the standard pattern of orthorhombic V_2O_5 powder (a_0 = 1.1516 nm, b_0 = 0.3565 nm, c_0 = 0.4372 nm; SG = Pmnm, JCPDS 41–1426). The $V_2O_5 \cdot 1.5H_2O(HDA)_{0.7}$ (Figure 3(b)) exhibits a set of {00l} peaks characteristic of the formation of a bilayer laminar phase and evidence for the formation of a crystalline matrix. The interlaminar distance is measured to be 2.5 nm from the (001) Bragg reflection. By comparison, the interlaminar spacing of the monoclinic (a_0 = 1.1964 nm, b_0 = 0.4697 nm, c_0 = 0.5324 nm; space group = c2/c) $V_2O_5 \cdot nH_2O$ xerogel is calculated to be 1.27 nm from its respective (001) Bragg reflection (Figure 3(a)) and displays a lower degree of long-range laminarity. Nanotubes formed after HT are a pure mesophase formed by tubular species (*vide infra*) with interlaminar distances of ∼3 nm, shown in Figure 3(c).

X-ray powder diffraction patterns of the V_2O_5 nanotubes before and after pressing were also acquired. The ratio of the corresponding {00l} planes is shown in Figure 4. The patterns show that the intensity of the normalized (002) reflection decreases by a factor of ∼0.25 and increases by a factor of ∼6 before and after the V_2O_5 nanotubes have been pressed into parallelepipedal pellets, respectively, with respect to the initial vanadium oxide xerogel precursor.

The observation of the relatively intense (002) Bragg reflection in the compressed pill indicates a reduction in the degree of bilayer order of surfactant arrangement between vanadate layers, which normally results is the canceling of the (002) reflection [7]. This observation [12] may be ascribed to

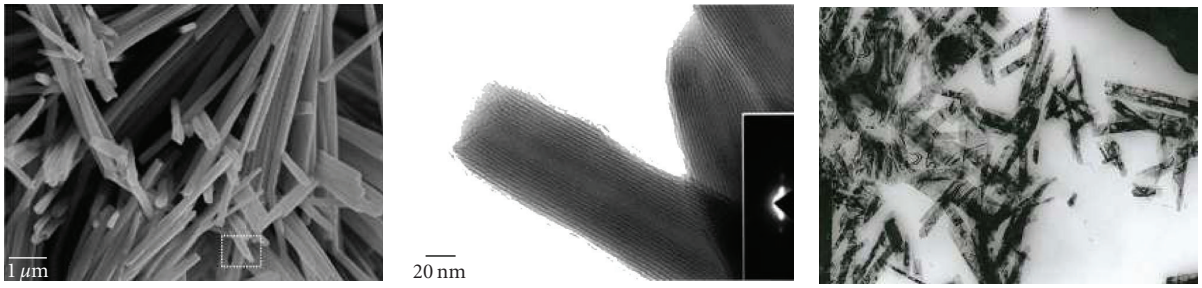

(a) (b) (c)

Figure 2: (a) FESEM image of a cluster of V_2O_5 nanotubes. (b) TEM image of a fully developed nanotube. Lattice planes are clearly resolved at the sidewall regions; the inset SAED pattern evidencing the 2.9 nm interlaminar spacing. (c) TEM image of multiple monocrystalline nanorods.

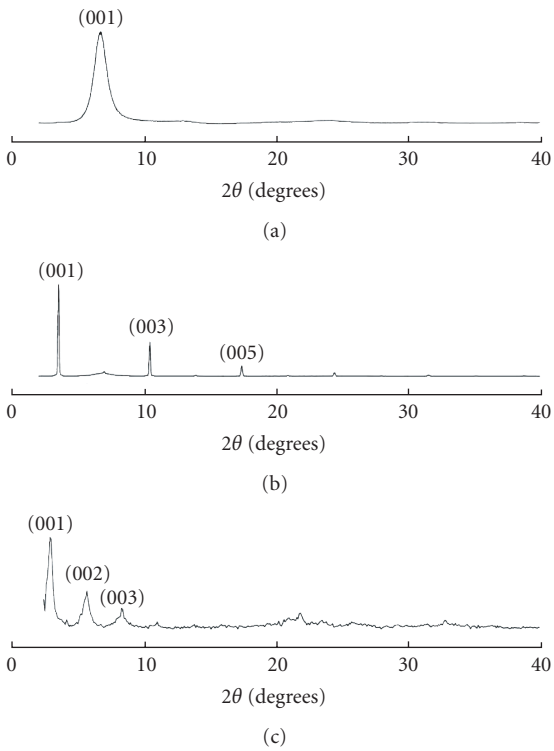

Figure 3: Normalized X-ray diffraction patterns of (a) $V_2O_5 \cdot xH_2O$ xerogel, (b) surfactant-intercalated xerogel, $V_2O_5 \cdot 1.5H_2O(HDA)_{0.7}$, and (c) post-HT V_2O_5 nanotubes.

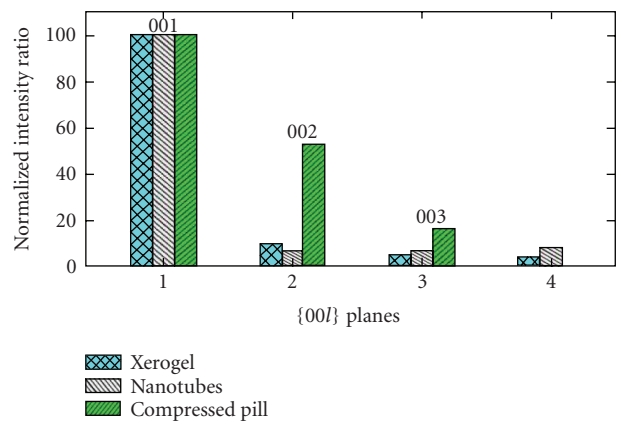

Figure 4: Comparison of normalized {00l} peak intensities derived from XRD patterns of the xerogel, nanotubes and compressed pills.

the existence of preferential longitudinal orientations of the intrinsically anisotropic nanotubes in the pellets [11], as can be seen in Figure 1.

Electrical conductivity measurements were also performed on compressed nanotube samples. Arrhenius plots, shown in Figure 5, exhibit a near-linear behavior in almost all cases, from which the activation energy, E_a, for the processes may be estimated. In the case of $\sigma_\perp$ (conductivity perpendicular to the pill surface), the slope of the Arrhenius plot is estimated to be ~0.15 eV, slightly lower than that of $\sigma_\parallel$ for which $E_a = 0.23$ eV. The conductivity in the nanotubes under an applied pressure of 2.3 MPa is about two orders of magnitude larger in the direction perpendicular to the applied pressure ($\sigma_\perp$) than is measured in the parallel direction ($\sigma_\parallel$) [11]. As expected, the conductivity varies exponentially with temperature and the Arrhenius plots always show, in the measured temperature range, a quasilinear dependency where $(E_{a\perp}/E_{a\parallel}) = 1.58$.

Four-point probe resistivity measurements on the surface of compressed-nanotube parallelepipedal pills containing $V_2O_5 \cdot 0.6H_2O(HDA)_{0.69}$ revealed a semiconducting behavior with a resistivity of ~200 Ω cm, an improvement of a factor of ~3 over recent findings [13], although it must be highlighted that no indication of the applied pressure in previous reports was made.

These results conclude that electrical conductivities in compressed nanotubes at room temperature are of the order of $\sigma_\perp \simeq 10^{-3}$ S cm^{-1} and $\sigma_\parallel \simeq 10^{-6}$ S cm^{-1}. To rationalize the anisotropy values, the nanotubes must be oriented preferentially in the parallel to the tube axis (*vide supra*) as the surface resistivity of the nanotubes perpendicular to the long axis of the tubes is much greater (~600 Ω cm). The degree of anisotropy, α, can thus be defined as the ratio of perpendicular and parallel conductivities ($\alpha = \sigma_\perp/\sigma_\parallel$). As a function of temperature, the anisotropy after pressing at 2.3 MPa is measured at $\alpha = 70$ at 298 K decreasing to a value

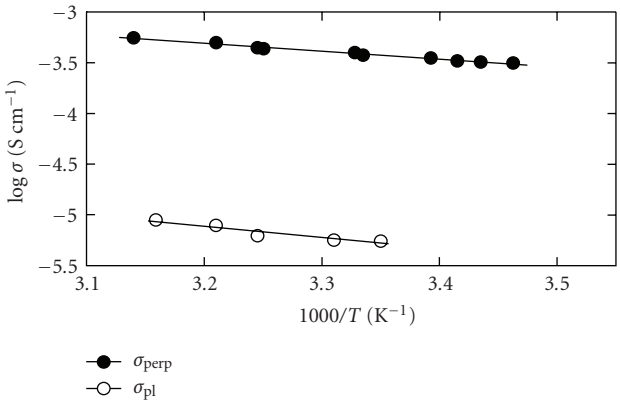

Figure 5: Conductivity measured as function of temperature for the compressed pill of VOx nanotubes (– ∘ –) parallel and (– • –) perpendicular to the direction of applied pressure.

of $\alpha = 55$ at 313 K. This temperature-dependent reduction of the degree of anisotropy is due to the decomposition and/or associated conformational change of the amine-intercalated V_2O_5 nanotubes [10].

3.2. Electrochemical measurements with V_2O_5 nanostructures

In comparison with other tubular systems, the VOx nanotubes and associated nanostructures are especially interesting from the point of view of ion intercalation because they possess four different contact regions, that is, tube opening, outer surface, inner surface, and interstitial regions.

Electrochemical experiments reproducing both the discharge and the incremental charge capacity curves for the intercalation of lithium into V_2O_5 nanotubes at room temperature from 3.00–2.64 V are illustrated in Figures 6(a), 6(b), and 6(c), respectively. Pseudoequilibrium potential values in the lithium mole fraction range $0 \leq x \leq 0.65$, shown in Figure 6(a), correspond to an uptake of 0.65 Li/V_2O_5. The maximum charge capacity is 1225 mAh g^{-1}, an improvement of a factor of ~4.5 over thin film electrodes (260 mAh g^{-1}), and it is observed to decrease to 90% of this value after 25 charge/discharge cycles. A characteristic feature of the voltage-composition curve in Figure 6(a) is the relatively steady voltage observed in the 0–0.2 and 0.4–0.6 ranges of x.

Three inflection points in the open-circuit voltage are observed at around $x = 0.1$, 0.3, and 0.5. These inflection points can be clearly observed as maxima at $x = 0.1$, 0.3, 0.5 in the incremental charge capacity shown as a function of potential versus Li_x mole fraction curve in Figure 6(b). Continuous discharge curves are reported by some authors, while others observe several steps, as seen in Figure 6(a). These discrepancies have been related to the hydration state of vanadium pentoxide ranging from $n = 0.3$ up to $n = 2.2$ ($n = 1.5$ in this work). The presence of water of other solvent molecules in the gel leads to a more ordered stacking of the vanadate layers [7, 14], and furthermore, the high volumetric structures negate the need for precisely controlled interlaminar distances and hydration states of the vanadate lamina.

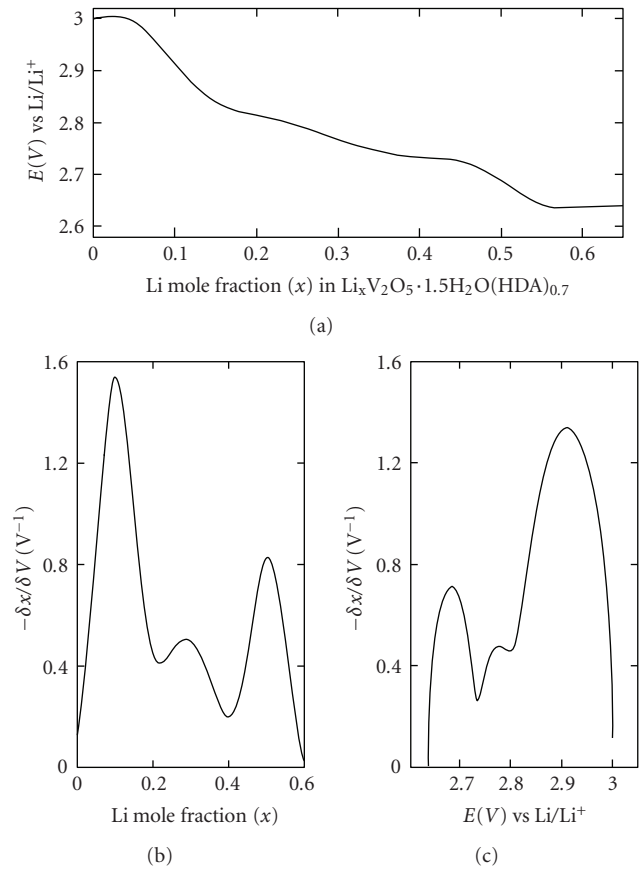

Figure 6: (a) Quasiequilibrium voltage-composition curve for the intercalation of lithium into $V_2O_5 \cdot 1.5H_2O(HDA)_{0.7}$. (b) Relative incremental capacity as function of lithium concentration in the mole fraction range $x = 0.0$–0.65. (c) Relative incremental capacity as function of discharge voltage during lithium intercalation.

α-$Li_xV_2O_5$ is the phase formed when only a small amount of lithium is intercalated; the thermodynamic stability interval is $0 \leq x \leq 0.1$, as seen in Figure 6. The peak corresponding to the lithium mole fraction $x = 0.1$ in the $Li_xV_2O_5 \cdot 1.5H_2O(HDA)_{0.7}$ nanotubes represents the formation of α-$Li_xV_2O_5$. The single phase transition to β-$Li_xV_2O_5$ is thus observed at the inflection point $x = 0.3$, shown in Figure 6(b). The sharpness of the peak indicates an abrupt phase transition, occurring over a voltage range of ~60 mV versus Li/Li^+, as shown in Figure 6(c). The β-$Li_xV_2O_5$ formed during lithium intercalation has the widest measured thermodynamic composition interval, observed from Figure 6(a) to be in the range $0.15 \leq x \leq 0.45$ [15]. It has a tunnel-like structure with a number of possible sites for insertion of lithium ions.

Two different β-$Li_xV_2O_5$ modifications are know (β and β'), differing with respect to the sites occupied by lithium ions. The peak seen in Figure 6(a) at $x = 0.3$ corresponds to the β-phase.

The vanadium-oxygen framework is kinetically stable towards transitions to α- or β-phases, whereas the $\beta \Leftrightarrow \beta'$ transition observed at $x = 0.5$, which only involves a displacement of mobile lithium ions, readily occurs. Thus, the prominent inflection point at $x = 0.5$ in Figure 6(c) is due to the ready formation of the β'-$Li_xV_2O_5$ phase of the lithiated vanadate.

Our recent successful synthesis of highly turbostratic vanadate nanofibers using thiols rather than amines was also studied from the point of view of electrochemical lithiation under identical conditions. The trace amount of sulfur from the thiol headgroups is thought to exert a catalytic influence on Li^+ integration [16]. However, the formation of Li_2S_n polysulfides was not observed nor was the characteristic $Li_2S_n \rightarrow Li_2S$ transformation at 1.8 V versus Li/Li^+. There is, furthermore, no evidence from either the diffraction or electrochemical data of the presence of Li_2O in the hydrated vanadate nanostructures after extensive charge/discharge cycling.

The improved electrochemical properties observed in novel vanadium oxide nanostructured arrays are attributed to the increased volumetric density for ion intercalation, shorter diffusion paths to the intercalation sites, and high degree of crystallinity of the individual nanotubular host structures. In addition, these anisotropic structures permit the greatest freedom for dimensional change that accompanies intercalation and extraction reactions and enhance Li^+ diffusion through the solvent. The high degree of long-range uniformity and crystallinity aids in kinetic charge transport characteristics by minimizing the influence of grain boundary effects more often observed in thin-film electrodes. Furthermore, the shortened diffusion distance reduces the Li^+ insertion rate density per unit area and, consequently, concentration polarization within the electrode during the discharge process is prevented.

ACKNOWLEDGMENTS

The support of the Science Foundation Ireland (SFI) under investigator award 02/IN.1/172, the Network of Excellence P*h*OREMOST, the University of Chile, the Universidad Tecnológica Metropolitana, and FONDECyT Grants 1050344, 1030102, 7050081, 1050788 are gratefully acknowledged.

REFERENCES

[1] R. Schöllhorn, *Physics of Intercalation Compounds*, Springer, Berlin, Germany, 1981.

[2] M. S. Whittingham, "Lithium batteries and cathode materials," *Chemical Reviews*, vol. 104, no. 10, pp. 4271–4302, 2004.

[3] M. E. Spahr, P. Stoschitzki-Bitterli, R. Nesper, O. Haas, and P. Novák, "Vanadium oxide nanotubes. A new nanostructured redox-active material for the electrochemical insertion of lithium," *Journal of the Electrochemical Society*, vol. 146, no. 8, pp. 2780–2783, 1999.

[4] Y. Wang and G. Z. Cao, "Synthesis and enhanced intercalation properties of nanostructured vanadium oxides," *Chemistry of Materials*, vol. 18, no. 12, pp. 2787–2804, 2006.

[5] Y. Wang, K. Takahashi, K. H. Lee, and G. Z. Cao, "Nanostructured vanadium oxide electrodes for enhanced lithium-ion intercalation," *Advanced Functional Materials*, vol. 16, no. 9, pp. 1133–1144, 2006.

[6] V. Lavayen, C. O'Dwyer, M. A. Santa Ana, et al., "Comparative structural-vibrational study of nano-urchin and nanorods of vanadium oxide," *Physica Status Solidi B*, vol. 243, no. 13, pp. 3285–3289, 2006.

[7] C. O'Dwyer, V. Lavayen, S. B. Newcomb, et al., "Atomic layer structure of vanadium oxide nanotubes grown on nanourchin structures," *Electrochemical and Solid-State Letters*, vol. 10, no. 4, pp. A111–A114, 2007.

[8] C. O'Dwyer, D. Navas, V. Lavayen, et al., "Nano-urchin: the formation and structure of high-density spherical clusters of vanadium oxide nanotubes," *Chemistry of Materials*, vol. 18, no. 13, pp. 3016–3022, 2006.

[9] V. Lavayen, C. O'Dwyer, G. González, G. Cárdenas, and C. M. Sotomayor Torres, "Towards thiol functionalization of vanadium pentoxide nanotubes using gold nanoparticles," *Materials Research Bulletin*, vol. 42, no. 4, pp. 674–685, 2007.

[10] C. O'Dwyer, V. Lavayen, S. B. Newcomb, et al., "Vanadate conformation variations in vanadium pentoxide nanostructures," *Journal of the Electrochemical Society*, vol. 154, no. 8, pp. K29–K35, 2007.

[11] V. Sánchez, E. Benavente, V. Lavayen, et al., "Pressure induced anisotropy of electrical conductivity in polycrystalline molybdenum disulfide," *Applied Surface Science*, vol. 252, no. 22, pp. 7941–7947, 2006.

[12] V. Lavayen, N. Mirabal, C. O'Dwyer, et al., "The formation of nanotubes and nanocoils of molybdenum disulphide," *Applied Surface Science*, vol. 253, no. 12, pp. 5185–5190, 2007.

[13] H.-J. Muhr, F. Krumeich, U. P. Schönholzer, et al., "Vanadium oxide nanotubes—a new flexible vanadate nanophase," *Advanced Materials*, vol. 12, no. 3, pp. 231–234, 2000.

[14] Y. Wang, H. Shang, T. Chou, and G. Z. Cao, "Effects of thermal annealing on the Li^+ intercalation properties of $V_2O_5 \cdot nH_2O$ xerogel films," *Journal of Physical Chemistry B*, vol. 109, no. 22, pp. 11361–11366, 2005.

[15] K. West, B. Zachau-Christiansen, T. Jacobsen, and S. Skaarup, "Lithium insertion into vanadium pentoxide bronzes," *Solid State Ionics*, vol. 76, no. 1-2, pp. 15–21, 1995.

[16] K. Lee, Y. Wang, and G. Z. Cao, "Dependence of electrochemical properties of vanadium oxide films on their nano- and microstructures," *Journal of Physical Chemistry B*, vol. 109, no. 35, pp. 16700–16704, 2005.